Ta-DAH: Task Driven Automated Hardware Design of Free-Flying Space Robots

Lucy Jackson, Celyn Walters, Steve Eckersley, Mini Rai and Simon Hadfield

Abstract—Space robots will play an integral part in exploring the universe and beyond. A correctly designed space robot will facilitate OOA, satellite servicing and ADR. However, problems arise when trying to design such a system as it is a highly complex multidimensional problem into which there is little research. Current design techniques are slow and specific to terrestrial manipulators. This paper presents a solution to the slow speed of robotic hardware design, and generalizes the technique to free-flying space robots. It presents Ta-DAH Design, an automated design approach that utilises a multi-objective cost function in an iterative and automated pipeline. The design approach leverages prior knowledge and facilitates the faster output of optimal designs. The result is a system that can optimise the size of the base spacecraft, manipulator and some key subsystems for any given task. Presented in this work is the methodology behind Ta-DAH Design and a number optimal space robot designs.

Keywords—Space robots, automated design, on-orbit operations, hardware design

I. Introduction

FROM the development of the first space-based manipulator in 1981, to the more recent development of the Perseverance Mars Rover, robotic technologies have always been, and will likely remain an integral part of space exploration. An area of space robotics which is gaining interest is On-Orbit Assembly (OOA). Driven by curiosity, humans are continually trying to put larger and larger structures in space. However, the size of launch vehicle fairings and testing facilities on Earth has impaired progress. One approach to this problem is to develop larger launch vehicles. Another suggested solution is the idea of OOA. Until recently the idea of OOA has been limited to large national missions, such as the assembly of The International Space Station (ISS), with bespoke components and oversized robotics. However, a new space era is approaching in which low-cost, innovative, intelligent and autonomous robotic assembly systems are commercially viable and applicable to smaller missions and a wider market. To date, the design of space robotics within this category has rarely been explored.

It is known that orbital robotics have the capability to achieve missions beyond OOA. Potential tasks include but are not limited to Active Debris Removal (ADR), refueling, part repair or replacement and other servicing missions. All of these tasks fall under the umbrella of On-Orbit Operations (OOO). A robotic system capable of carrying out OOO will likely be one or more manipulators mounted on a base spacecraft, known as a space robot — a representation of this can be seen in Figure 1. Note that the manipulator can have any number of Degrees of Freedom (d.o.f.), in this research only the single arm system is evaluated.

Fig. 1: A space robot is defined as a manipulator of any number of d.o.f. mounted on a base spacecraft of any size.

At present, there are only a handful of space robots that are capable of operating on-orbit. All of those which can are bespoke systems that have been designed for a specific mission objective or technology demonstration. This limits their versatility and reusability. Designing a small, more robust, space robot would provide a wealth of benefits. Smaller systems will mean tasks can be conducted in smaller, confined spaces, increasing their flexibility. Smaller systems will also be much more likley to fit on a 'piggy back' launch, making them easier and cheaper to deploy versus their heavier counterparts. However, systems of reduced size will be less capable of manipulating large payloads and will be more susceptible to instabilities due to the increased effect of dynamic coupling. Dynamic coupling occurs as a result of the micro-gravity operating conditions and means that any forced motion of the manipulator or base will induce a force in the other component. It is this phenomenon that causes the biggest issues when trying to operate a space robot in-situ.

Current approaches to the design of such systems involve trial-and-error prototyping evaluated by performance in the target task. This results in individual solutions following a costly,

L. Jackson (ljackson@surrey.ac.uk), C. Walters (celyn.walters@surrey.ac.uk) and S. Hadfield (simon.hadfield@surrey.ac.uk) are at CVSSP, University of Surrey

M. Rai (mrai@lincoln.ac.uk) is with the School of Engineering at the University of Lincoln

S. Eckersley (SEckersley@sstl.co.uk) is with Surrey Satellite Technology Ltd., Tycho House, Guildford

time and resource intensive process. In an attempt to combat this, designs for different agents with a similar or identical function can be modified and updated as opposed to needing to restart the Research and Development (R&D) process. This process was followed with the Mars rovers designed by National Aeronautics and Space Administration (NASA). To date, NASA has successfully operated 5 rovers on Mars; Sojourner, Spirit, Opportunity, Curiosity and Perseverance. While the overall design of the rovers stayed consistent, modifications and improvements were made to different components — for example, the size of the wheels increased incrementally from the first to the last design. This 'heritage' approach to the physical design of robots speeds up the R&D process and lowers costs, allowing for a higher level of technology transfer and 'learning from mistakes'. However, the design process still remains expensive and time-consuming, relying on laborious manual design techniques. Even with prior knowledge, the development of Perseverance took 11 years and cost upwards of $\$2.4$ million [23].

This paper presents Task Driven Automated Hardware Design (Ta-DAH Design), an automated design technique that will aid in cutting costs and lead times for free-flying space robot missions. Ta-DAH Design removes the need to manually produce, evaluate and test different space robot design options. The proposed automated design process encodes and leverages prior knowledge in a compact and meaningful way. In particular, Ta-DAH Design is set-up to modifying and updating certain design parameters of a successful predecessor robot. In addition to improving the R&D process, there is potential for the successful implementation of this automated design technique to actually improve the overall performance of an agent. This would be possible by finding a more optimal design that would not have been discovered via systematic human-in-the-loop iteration.

This work contains three main contributions:

1) A novel multi-objective cost function is defined and used with a weighted sum approach to optimise the hardware of a free-flying space robot.
2) Ta-DAH Design is presented in a user-friendly toolbox. It is believed to be the first piece of software of its kind. All code is availabile at https://gitlab.surrey.ac.uk/lj00304/Ta-DAH.
3) The definition of a number of different space robot designs, where each is optimal for a different task.

The rest of this paper is organised as follows. The next section highlights seminal work in the field of hardware design and relevant past missions. Next, the methodology of Ta-DAH Design is outlined. The results are then discussed in the following section before the conclusions and future work are given.

II. Related Work

A. Past Missions

A number of agencies have used robotic technologies in space, not just in the form of free-flyers but also humanoids, semi-humanoids and large manipulators. Table I provides an extensive list of current and planned robotic missions. It should be pointed out that with the emergence of many new space companies there maybe planned missions that have not been publicised at the time of writing.

Table I highlights the lack of free-flying 'heritage' techonologies, with only two successful missions. In addition to this, looking at all the missions, the large size of current robotics becomes apparent. The most recent advance in the state-of-the-art against this trend is the Kraken manipulator [37]. This is a commercial project developed by Tethers unlimited, which proposes a 4.2kg, 7 d.o.f. manipulator. However, no further information in relation to the sizing of individual links or the base spacecraft onto which it will be mounted are avaliable. In addition to this, no performance metrics or operating conditions of the system could be found and it is unclear if development has moved beyond feasability studies.

B. Hardware Design

While there are a number of papers presenting the final design of space robots, very few give substantial information on the design process. [20] give details on how the design of a small 11 d.o.f. system was reached, although this approach is not general or applicable to other tasks. They present a method that evaluated three different manipulator configurations and selected the best one for their particular use case. Contary to this, Ta-DAH Design is a generic method whereby a design for any specified task can be generated.

Available in the literature however, is a wealth of information on the techniques used to design *terrestrial* robots. [3], [17] and [22] all provide optimisation techniques for such manipulators, where a method is provided for a system with three d.o.f. [17] uses the condition number of the Jacobian matrix to find the optimal link lengths. [3] use a weighted multi-objective function consisting of task-time and joint torques to optimise the robots trajectory, link lengths and mass, subject to kinematic and dynamic constraints. [22] proposed a method to maximise a robot's workspace within performance constraints. The drawback of all of these techniques is that they are only applicable to low d.o.f. systems. If any of these methods were to be directly utilised in the context of this work, they would need to be scaled up, drastically increasing complexity by a power of 4.

[21] presents a more scalable method applied to a 6 d.o.f. manipulator. It consists of finding the configuration that leads to the minimal error between the end effector position and a number of task points. However, this approach is dependent on an overarching workspace constraint and a clear definition of a number of task points. This becomes redundant in the case of a space robot since its workspace is unconstrained. [6] proposed a design method that instead approaches the problem from a subsystem level, therefore requiring less specific task knowledge. They reduced the problem into one involving non-continuous variables. This was done by parameterising the design into a number of modules (*i.e.* motors, sensing, frames), each with a performance and cost value. Each design was then optimised by subtracting cost from performance. Improvement of their method would involve the introduction of continuous variables.

TABLE I: Summary of launched and planned space robotic technology missions [1], [10]–[12], [15], [16], [18], [24], [25], [28], [30], [32], [33], [37].

Name	Launch Date	Stage	Type of mission	Mass (kg)
SRMS	1981	Operating off the ISS	Manipulator	431
ROTEX	1993	No longer in operation	Manipulator	-
ETS-VII	1997	No longer in operation	Free-flyer	2540
SSRMS	2001	Operating off the ISS	Manipulator	1497
DART	2005	Failed in flight	Free-flyer	-
Orbital Express	2007	No longer in operation	Free-flyer	1090
DEXTRE	2008	Operating off the ISS	Semi-humanoid	1560
Robonaut 2	2011	Returned to Earth in 2018	Humanoid	150
ERA	2012	Operating off the ISS	Manipulator	630
DEOS	-	Program canceled	Free-flyer	-
FREND	-	Suggested for use on a number of missions	Manipulator	78
TALISMAN	-	No launch date	Manipulator	36.2
KRAKEN*	-	No launch date	Free-flyer	4.2
Next Generation Canadarm	-	Announced 2013	Manipulator	-
SPIDER	-	Developed for OSAM-1 Mission	Manipulator	-
VISPA*	-	Developed by Airbus	Manipulator	14.5

*Commercial project

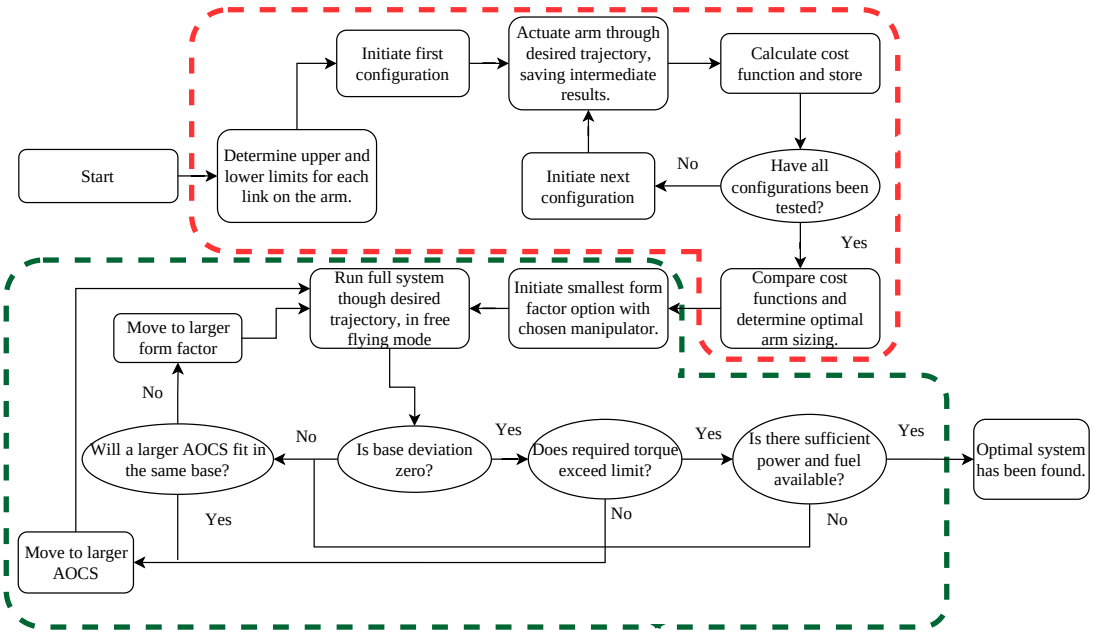

Fig. 2: The full optimisation process for the space robot is shown here. Highlighted in red is the section that relates to the optimisation of the arm while the green part highlights the base optimisation procedure. Each part is expanded and explained in the following section.

The majority of literature in the field approaches the optimisation of terrestrial robots using a multi-objective cost function [29], [34], [41]. A multi-objective optimisation problem is defined as a collection of conflicting objective functions which are addressed systematically and simultaneously [7]. There exist many approaches to solving multi-objective problems. The issue when solving such a problem comes from the fact that the search space becomes partially ordered. Pareto fronts are not necessarily convex, meaning solutions may be locally optimal as opposed to globally optimal [2]. Extensive research has been done into methods to solve the optimisation problem, with a number of summaries available in the literature [8], [14], [26]. According to [26], these can be categorised into 3 groups, those that require information as an input (*priori articulation*), those that require the user to select from a number of optimal designs (*posteriori articulation*) and those that require no user input (*no articulation of preferences*). This paper will focus on *Priori articulation* methods since the required input information can be inferred from desired tasks, *i.e.* if a system is required to assemble mirror segments it should have a reach of approximately 0.5 m and base stabilisation will occur prior to payload manipulation.

III. Methodology

The Ta-DAH Design optimisation approach for the space robot hardware is a two-step process. The first step looks at the size of the manipulator and the second at the size of the base. The optimisation is carried out in simulation. Figure 2 shows the full process. The size of the manipulator is determined using a constrained weighted sum optimisation approach, where constraints are set by user inputs and the target tasks. The process works by actuating the robotic manipulator through a trajectory and calculating the corresponding cost function. This is done for the full range of potential manipulator configurations within an allowable limit which is constrained by overall reach. The optimal configuration is then the one with the lowest cost function. Using this approach as opposed to an automated optimisation technique avoids local minimuma as all options are evaluated. However, the drawback is increased compuational time. At present, the process is not capable of optimising over d.o.f. so instead three different options are evaluated, and their final performance is compared.

Once the size of the manipulator has been optimised, the size of the base spacecraft is determined. This is done by mounting the chosen manipulator on the smallest form factor and evaluating its performance. Performance evaluation is done against a number of conditions and if all are met then the form factor in question is deemed to be the correct one, if not, the next size form factor is evaluated. This design approach puts emphasis on outputting the smallest operational system possible.

Both stages of the optimisation require the full dynamic model of the system, which was implemented in Matlab following the derivation presented in [35]. The model uses the reference frames shown in Figure 3. Each link has a reference frame at its joint ($\sum l_i$), which is used to define the rotation of that d.o.f./link. Rotations and translations of the base are measured by the movement of $\sum B$ w.r.t. an inertial reference frame ($\sum I$).

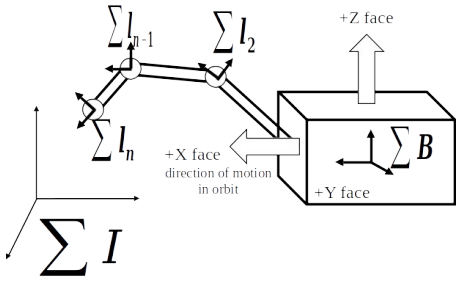

Fig. 3: The base position is defined as a movement of $\sum B$ w.r.t. $\sum I$. While the position of each link is described by the rotation of $\sum l_i$, which is fixed to the base of the corresponding link. Also shown here is the definition of the base spacecraft faces.

Evaluation is carried out with 6 tasks, that are defined in the next section. In this design approach there is no integrated controller so a Proportional Integral Derivative (PID) controller is used to control the system. This controller works by outputting the required control forces to reduce the error between the current and desired state of the system. In order to implement this controller, a desired trajectory is needed. This is generated using an initial and final configuration for each task. A high order polynomial is then used with the inverse kinematics of the system to resolve the desired joint at each time step in the simulation.

A. Arm Optimisation

The principle of the weighted sum objective optimisation problem is to determine a number of parameters in order to minimise a cost function $\mathcal{C}$, where

$$\mathcal{C} = \sum_{i=1}^{j} \mathbf{w}_i \mathcal{F}_i \left(\mathbf{v}^*\right). \tag{1}$$

Here, $\mathbf{v}^*$ is a design vector, $\mathcal{F}_i$ represents each objective function, and $\mathbf{w}_i$ is the weight given to the corresponding function. In this context, the design vector is defined as

$$\mathbf{v}^* = \begin{bmatrix} \mathrm{l}_1 & \mathrm{l}_2 & \dots & \mathrm{l}_{\mathrm{n}_m} \end{bmatrix}^T, \tag{2}$$

where $\mathrm{l}_{1..\mathrm{n}_m}$ represents the length of each link in the manipulator, and n_m the total number of links on the manipulator. The same joint configuration is adapted for use with a manipulator of any d.o.f. Other than joint 1, joints provide rotation about the link's *z-axis* and additional d.o.f. are added prior to Joint n-1. Joint 1 however, rotates about its *x-axis* in order to increase the manipulators' reach.

The objective functions selected aim to represent the parameters necessary for the successful operation of the space robot. These are summarised in Table II and are discussed and formalised in turn.

1) Objective 1: Objective function one ($\mathcal{F}_1$) relates to the system's pseudo-workspace. Workspace is not directly considered since, due to their nature, space robots have the potential to possess an unlimited workspace [13]. While this

TABLE II: All the objective functions used to optimise the space robot mainpulator.

	Definition
$\mathcal{F}_1\ (\mathbf{v}^*)$	Reach of the Manipulator
$\mathcal{F}_2\ (\mathbf{v}^*)$	Manipulability of the manipulator configuration
$\mathcal{F}_3\ (\mathbf{v}^*(\mathrm{t}))$	Error between the CoM of the end effector and the desired location
$\mathcal{F}_4\ (\mathbf{v}^*(\mathrm{t}))$	Forces and torques applied to the base during arm actuation
$\mathcal{F}_5\ (\mathbf{v}^*(\mathrm{t}))$	Torque required at each joint to move the arm at a given velocity and acceleration

is not strictly true and an 'attitude confined' workspace can be defined, this becomes a function of the path history, and therefore the selected orbit [36]. This means the orbit of the same system could be altered to satisfy workspace demands. As a result, workspace should only ever be considered as a 'soft' constraint. The overall reach of the manipulator will be considered instead, since this governs the area alongside the orbit that can be reached by the spacecraft. The reach puts constraints on the close proximity and rendezvous capability. $\mathcal{F}_1(\mathbf{v}^*)$ is the sum of the link lengths, which in this case is the sum of the design vector components,

$$\mathcal{F}_1\left(\mathbf{v}^*\right) = \sum_{i=1}^{\mathrm{n}_m} \mathrm{l}_i. \tag{3}$$

2) Objective 2: Manipulability is a measure of the capability of a robot to execute a specific task in a given configuration, and this attribute governs objective function 2. This quantifies the ability of a manipulator to move and orientate its end effector within a given workspace. This value is still useful for space robots, even with their undefined workspace, since it is based on dexterity and the prevalence of singularities within the workspace as opposed to the size of the workspace itself. $\mathcal{F}_2(\mathbf{v}^*)$ is defined as

$$\mathcal{F}_2\left(\mathbf{v}^*\right) = \sqrt{det\left[\mathbf{J}\left(\mathbf{v}^*, \mathbf{q}\right)\mathbf{J}\left(\mathbf{v}^*, \mathbf{q}\right)^T\right]}. \tag{4}$$

$\mathbf{J}$ is the Jacobian of the manipulator and $\mathbf{q}$ is the state vector of the system. This is defined as $\mathbf{q} = \begin{bmatrix}\mathrm{x} & \mathrm{y} & \mathrm{z} & \alpha & \beta & \gamma & \theta_1 \cdots \theta_{\mathrm{n}_m}\end{bmatrix}^T$. The first 3 terms represent the linear position of the base $(\mathrm{x}, \mathrm{y}, \mathrm{z})$ and the next 3 terms represent the attitude of the base (α, β, γ). $\mathcal{F}_2(\mathbf{v}^*)$ is dependent on the manipulator's instantaneous position. In each case this will be calculated for the final position of the manipulator.

3) Objective 3: The error between the Center of Mass (c.o.m) of the end effector and the desired location, defined by the task, will also contribute to an objective function. This is because it quantifies the error in the manipulator's positioning. $\mathcal{F}_3\ (\mathbf{v}^*(\mathrm{t}))$ is therefore initially defined as

$$\mathcal{F}_3\left(\mathbf{v}^*\left(\mathrm{t}\right)\right) = \mathcal{I}_{d_t} - \mathcal{I}_a\left(\mathbf{v}^*\left(\mathrm{t}\right)\right). \tag{5}$$

$\mathcal{I}_a$ is used to represent the inverse kinematics of the actual position of the system, and $\mathcal{I}_d$, the desired position of the system. This objective function is time-dependent. This should be avoided as it adds another level of dimensionality to an already complex problem. As a result, it is instead re-defined to capture the worst case value for the given trajectory,

$$\mathcal{F}_3\left(\mathbf{v}^*\right) = \max_{\mathrm{t}}\left[\mathcal{I}_{d_t} - \mathcal{I}_a\left(\mathbf{v}^*\left(\mathrm{t}\right)\right)\right]. \tag{6}$$

4) Objective 4: Pivotal to the performance of the space robot is its ability to remain stable throughout operation. The effect of dynamic coupling can be quantified by looking at the torques and forces applied to the base spacecraft during arm actuation. This will be used as objective function 4 which is defined as

$$\mathcal{F}_4\left(\mathbf{v}^*(\mathrm{t})\right) = \left[\mathbf{D}\left(\mathbf{v}^*(\mathrm{t})\right)\ddot{\mathbf{q}} + \mathbf{C}\left(\mathbf{v}^*(\mathrm{t})\right)\dot{\mathbf{q}}\right]_{1:6}. \tag{7}$$

The subscript $_{1:6}$ denotes that only the forces applied to the base are in question here, *i.e.* the first 6 elements of $\boldsymbol{\tau}$, where $\boldsymbol{\tau} = \mathbf{D}\ddot{\mathbf{q}} + \mathbf{C}\dot{\mathbf{q}}$. The velocity of each element in the state vector is defined as $\dot{\mathbf{q}} \in \mathbb{R}^n$ and $\ddot{\mathbf{q}} \in \mathbb{R}^n$, are the corresponding accelerations. Where n quantifies the total d.o.f. of the space robot. The $\mathbf{D} \in \mathbb{R}^{n\times n}$ matrix represents the inertial properties of the system, and $\mathbf{C} \in \mathbb{R}^{n\times n}$ the Coriolis properties. As with objective function 3, $\mathcal{F}_4(\mathbf{v}^*(\mathrm{t}))$ is time-dependent and must be modified to account for the total effect of the dynamic coupling throughout the manipulator's trajectory:

$$\mathcal{F}_4\left(\mathbf{v}^*(\mathrm{t})\right) = \sum_{\mathrm{t}=0}^{\mathrm{T}}\left[\mathbf{D}\left(\mathbf{v}^*(\mathrm{t})\right)\ddot{\mathbf{q}} + \mathbf{C}\left(\mathbf{v}^*(\mathrm{t})\right)\dot{\mathbf{q}}\right]_{1:6}, \tag{8}$$

where t is the time step in the simulation and T is the total time for that task.

5) Objective 5: Due to the nature of the satellite, body mounted solar panels will be used. Combining this with the idea of making the system as small as possible presents the issue that power will be a finite resource. Power consumption is therefore considered when defining the objective functions. Objective function 5 $(\mathcal{F}_5\ (\mathbf{v}^*(\mathrm{t})))$ is defined as the mechanical power required to actuate the arm and its payload,

$$\mathcal{F}_5\left(\mathbf{v}^*(\mathrm{t})\right) = \left[\mathbf{D}\left(\mathbf{v}^*(\mathrm{t})\right)\ddot{\mathbf{q}} + \mathbf{C}\left(\mathbf{v}^*(\mathrm{t})\right)\dot{\mathbf{q}}\right]_{6:n}. \tag{9}$$

Again, this is time-dependent and as a results is modified to account for the total power required throughout actuation;

$$\mathcal{F}_5\left(\mathbf{v}^*(\mathrm{t})\right) = \sum_{\mathrm{t}=0}^{\mathrm{T}}\left[\mathbf{D}\left(\mathbf{v}^*(\mathrm{t})\right)\ddot{\mathbf{q}} + \mathbf{C}\left(\mathbf{v}^*(\mathrm{t})\right)\dot{\mathbf{q}}\right]_{6:n}. \tag{10}$$

6) Final Cost Function: It is necessary to normalise each of the objective functions. This is done prior to the summation to ensure they are non-dimensional, and equally weighted. If $\overline{\mathcal{F}_i}\left(\mathbf{v}^*\right)$ represents the normalised function then,

$$\overline{\mathcal{F}_i}\left(\mathbf{v}^*\right) = \frac{\mathcal{F}_i\left(\mathbf{v}^*\right)}{|\ \mathcal{F}_i\left(\mathbf{v}^*\right)_{\max}\ |}. \tag{11}$$

The maximum value $(|\ \mathcal{F}_i\left(\mathbf{v}^*\right)_{\max}\ |)$ corresponds to the maximum value for any configuration in the testing range, as opposed to the maximum within the specific trajectory. It should be noted that this produces an upper bound of 1, with no lower bound, also acting to scale the objectives. A normal weighted sum cost function contains a number of functions to minimise. However, in this case, some objective functions quantify characteristics to maximise, such as the

manipulability and reach. As a result, these objective functions are added to the final cost function instead of being subtracted. The final cost function for use in the optimisation is therefore defined as;

$$\mathcal{C} = -\mathbf{w}_1\overline{\mathcal{F}_1}\left(\mathbf{v}^*\right) - \mathbf{w}_2\overline{\mathcal{F}_2}\left(\mathbf{v}^*\right) + \mathbf{w}_3\overline{\mathcal{F}_3}\left(\mathbf{v}^*\right) + \mathbf{w}_4\overline{\mathcal{F}_4}\left(\mathbf{v}^*\right) + \mathbf{w}_5\overline{\mathcal{F}_5}\left(\mathbf{v}^*\right). \tag{12}$$

Setting all $\mathbf{w}_i = 1$ will give all the objective functions exactly the same governance over the results due to the normalisation. As such, this work does not alter the weightings, however it should be known that these can be tuned if a designer is looking for any particular quality from the system. For example, setting $\mathbf{w}_2 = 2$ will output a more dexterous robot of a bigger size for the same task.

B. Base Spacecraft Optimisation

The previous section illustrates how the optimisation of terrestrial robotic manipulators can be adapted for use with a space robot manipulator. However, no such techniques exist in regard to the sizing of the base spacecraft. Instead, a new approach is taken whereby the smallest size system that is capable of supporting the arm during successful operation is determined. The form factor can take a number of discrete sizes, unlike the manipulator which inhabits a continuous design space. The options considered in this work are shown in Table III. The automated approach taken here is to start with the smallest form factor, see if it supports the arm, and if not, try the next smallest size. This requires a clear definition of the requirements that make the system operational. Since the aim of this work is to design an optimal system for a given task, not to optimise a full mission concept, a number of conditions are excluded here, for example uplink and down link capability. It has been determined that the spacecraft will be operational if all the conditions in Table IV are met.

1) Condition 1: The first condition states that the Attitude and Orbit Control Subsystem (AOCS) should be able to maintain zero deviation of the base spacecraft. This means that throughout arm actuation it is able to apply the equal and opposite force that is induced by the dynamic coupling. This is reliant on the appropriate sizing of the AOCS for the chosen manipulator. A larger manipulator, in comparison to the base will increase the demand on the subsystem. The size of the base must also be considered since a smaller base will be unable to accommodate a more powerful AOCS. This condition will be checked by analysing the required torque for zero deviation and comparing it to what is available from the appropriately sized AOCS.

The torque required from the AOCS can be calculated based on the configuration of the reaction wheels in the spacecraft and the force needed to rectify the position of the base. If matrix $\mathcal{A}$ dictates the reaction wheel position in the spacecraft, and $\boldsymbol{\tau}_d$, the required torque in each axis, in $\mathrm{N\,m}$, then the torque required by each reaction wheel $\left(\mathbf{H}^R\right)$ can be calculated using

$$\mathbf{H}^R = \mathcal{A}\boldsymbol{\tau}_d. \tag{13}$$

If there is one reaction wheel mounted in each axis matrix $\mathcal{A}$ becomes

$$\mathcal{A} = \begin{bmatrix} 1 & 0 & 0 \\ 0 & 1 & 0 \\ 0 & 0 & 1 \end{bmatrix}, \tag{14}$$

and Equation 13 becomes

$$\mathbf{H}^R = \begin{bmatrix} \boldsymbol{\tau}_d^x & \boldsymbol{\tau}_d^y & \boldsymbol{\tau}_d^z \end{bmatrix}^T, \tag{15}$$

and can be used to determine the required torque for zero-deviation. This is compared to available hardware in order to determine if condition 1 can be satisfied with the current manipulator and base spacecraft pair. A number of subsystems are proposed for use, these are summarised in Table V. COTS components are selected in order to keep manufacturing costs to a minimum. The torque quoted can be applied in each of the three axes.

2) Condition 2: The second condition requires the spacecraft to generate sufficient power to operate all the required subsystems. The satellite will generate power using body mounted solar panels since deployable panels would limit the space in which the system could operate. The power available for each of the different form factors was calculated using the method outlined in [9]. It is assumed that the panels will be mounted on the $+/-Y$, $-X$ and the $+Z$ face, where the Y faces are perpendicular to the velocity vector and the $+Z$ face is space-facing — as seen in Figure 3. This leaves the forward-facing panel $(+X)$ free to mount the arm and the Earth-facing panel $(-Z)$ free to mount antenna and other required hardware. The spacecraft is assumed to be in a Geosynchronous Orbit (GEO) at around $35\,786\,\mathrm{km}$. The corresponding orbital average powers can be found in Table VI.

3) Condition 3: This condition specifies that the system must have sufficient fuel to facilitate zero-deviation during arm manouvers. This means that the propulsion system must be capable of outputting sufficient thrust, where $\boldsymbol{\tau}_d$ is the required thrust force in N. I_{sp} is the specific impulse of the fuel being used in $\mathrm{N\,s\,kg^{-1}}$ and m^f is the mass of fuel in kg that must be expelled.

$$\mathrm{m}^f = \frac{\boldsymbol{\tau}_d \mathrm{t}}{I_{sp}} \tag{16}$$

can be used to determine the required mass of fuel as dictated by the $\boldsymbol{\tau}_d$ required to keep the base spacecraft at zero deviation.

A solid fuel is not suitable for use as it cannot be throttled and therefore a variable control force cannot be applied. Instead, a liquid or gas fuel will be used as this can be throttled and re-started. Electric propulsion is also not considered due to the already high power demands of the system. A cold gas system was selected for use since it is small and simple to implement, the drawback of these systems is the lower I_{sp}, although this is not thought to be an issue since the demand on the subsystem will be relatively low. Information on the linear thrusters considered for use during optimisation can be found in Table VII.

TABLE III: The size of the base spacecraft is defined using the CubeSat standard. The form factor is the number of units used to make the base spacecraft. The dimensions are given here, where d_x, d_y and d_z are the width, height and depth of the base and m_{sc}, its mass. A mass range is given since this is hardware dependent.

Form Factor	$3U$	$6U$	$12U$	$18U$	$24U$	$27U$
m_{sc} (kg)	$4 < ... \leq 8$	$8 < ... \leq 16$	$16 < ... \leq 24$	$24 < ... \leq 30$	$30 < ... \leq 35$	$35 < ... \leq 40$
d_x,d_y,d_z (m)	$0.1, 0.1, 0.3$	$0.2, 0.1, 0.3$	$0.2, 0.2, 0.3$	$0.3, 0.2, 0.3$	$0.4, 0.2, 0.3$	$0.3, 0.3, 0.3$

TABLE IV: All the required operating conditions for the base spacecraft.

Condition	Description
1	Zero deviation during free-flying mode
2	Sufficient power is available for all subsystems
3	Sufficient fuel is avaliable

TABLE V: A number of Commerical Off-the-shelf (COTS) reaction wheels have been selected. Each have different torque and size properties [4], [5], [19], [27], [31].

System	Max Torque ($\mathrm{mN\,m}$)	Max Speed (R.P.M)	Required Form Form Factor
UniSat-7	3.7	7000	12
SatBus 4RW0	5.9	6500	12
RSI 12-75	90	7500	24
HoneyBee Robotics Microsat CMG	112	12000	24
Bradford RW	265	4000	27

IV. Results and Discussion

A. Optimisation Process

In this work, the Ta-DAH Design process was implemented in Matlab. It encodes the dynamic model for a free-flying space robot. The optimisation process was run for each of the different mission scenarios outlined in Table VIII. The corresponding trajectories are shown in the Appendix. Three different manipulator configurations are analysed — 5, 6 and 7 d.o.f. While the defined tasks may not be employed in the same way as in Table VIII, this gives a range of trajectories, reach and payload combinations. This means the resulting designs could be selected based on any of these requirements, even if the use case does not directly correspond to the named task.

The average time for the toolbox to run for each of the 6 missions are as follows: 5 d.o.f., $22s$; 6 Dof, $72s$; 7 d.o.f., $165s$. As expected, the system takes longer to run for higher d.o.f. configurations due to increased levels of complexity. It

TABLE VI: Average orbital power output by each of the form factors.

Form Factor	Average Power (W)
$3U$	4.76
$6U$	8.97
$12U$	9.52
$18U$	13.7
$24U$	17.9
$27U$	14.28

TABLE VII: A number of different cold gas linear thrusters have been considered for use. Some values are approximated [38]–[40].

	I_{sp} $\left(\mathrm{N\,s\,kg^{-1}}\right)$	Wet mass (g)	Max Power (W)
NASA's C-Pod Micro	40	1244	5
CuSP	70	690	11
AFRL Prop unit	70	1005	15

should be pointed out that within the current literature, there is no way of determining the correct d.o.f. for each specific space robotic mission. Hence, the initial hypothesis used in this work is that this choice should be made post-optimisation by analysing the output behavior of each configuration.

B. Sizing of Manipulator

The optimal link lengths and form factors for all missions are shown in Figure 4, where the missions are referred to by the numbers in Table VIII. Note that the form factors highlighted in red are the optimal ones, excluding the power consumption. This is discussed in more detail in the next section. Figure 4 shows a large variation in the optimal hardware for the different missions. Not only does the optimal hardware vary from mission to mission, but also within each mission for the different d.o.f. options. This is apparent in the overall reach of the manipulator. In almost all cases, with an increased d.o.f. for the same desired reach, the favored overall reach is lower. The largest disparity in length is seen in missions 3 and 4. In both cases the 7 d.o.f. manipulator was the shortest. The increased number of joints means that the overall power to actuate the arm will be higher, so to keep power consumption down the overall mass of the arm is kept to a minimum. This is because a larger mass means higher inertia, which requires more force to actuate. The increase in d.o.f. also means that the base spacecraft will experience increased reaction forces, resulting in larger base deviations. This will increase the pressure on the AOCS and can again be alleviated by having an arm with lower inertia.

C. Sizing of Base Spacecraft

Of more interest, and slightly unexpected, is the increased form factor in the case of missions 1, 4 and 6 for the 5 d.o.f. manipulator. This is surprising because it has been shown that increasing the d.o.f. of the manipulator leads to

TABLE VIII: Desired tasks and corresponding motions.

Mission	Task	Desired motion	Required Reach (m)	Payload Mass (kg)
1	Move an object	Large manipulator motion during base stabilisation	0.8	5
2	Assemble modules	Fine manipulator motion with stable base	0.5	5
3	Assemble parts	Small precise motion with stable base	0.5	3
4	Fuel tank replacement	Large motion of end effector during base stabilisation	0.6	5
5	Part repair	Large motion of end effector with stable base	0.4	3
6	Debris removal	Smaller motion of arm during base stabilisation	0.8	5

an increase in power consumption and larger forces applied to the base spacecraft. It was therefore expected that the systems in need of an increased form factor would be the ones with a higher d.o.f. manipulator. This is because the larger form factor spacecraft provides a bigger surface area for power generation and can accommodate a higher specification AOCS. This surprising result was investigated further. It was found that the control algorithm employed was unable to stabilise the system for this configuration in the three missions in question, therefore requiring a larger form factor with increased AOCS capability. Re-running the same mission with no base motion led to the system operating as expected with the recommended form factor falling back to 12U. It would also be possible to stabilise the system using a bespoke control algorithm. This is a prime example of how a very small variation in the mission scenario can result in different optimal hardware or the required control technique.

D. Fuel and Power

Figure 5 shows the fuel and power demands for all manipulator types in each of the different mission scenarios. The trends in the fuel consumption mirror what was expected. It can be seen that there is a large increase in both the power and fuel requirements when base movement is required in the manoeuvre (missions 1, 4 and 6). In fact, for these missions, and the 7 d.o.f. design in mission 5, no form factor could provide sufficient power — highlighted in red in Figure 4. Although this was set as a condition for base optimisation, it was found that for these missions, none of the form factors could provide sufficient power. As such this condition was removed from the optimisation for these missions and the form factor was optimised independently of this — explaining why the maximum form factor is not selected for all the missions in question. Instead, a battery will be used to supplement power generation during these missions.

Figure 5 shows that fuel consumption for the 5 and 7 d.o.f. manipulators is consistently higher than for the 6 d.o.f. manipulator. This is due to the fact that in all missions, the 6 d.o.f. manipulator configuration was stable, whereas the 5 and 7 d.o.f. manipulator configurations were unstable. This means extra fuel and power was expended later in the mission. The instability of the 7 d.o.f. manipulator system was expected due to the increase in complexity needing further tuning of the control parameters or the use of a more robust algorithm. However, the instability of the 5 d.o.f. system was unexpected. This highlights the need for hardware and software optimisation to be considered simultaneously, somthing that has not been done in this research.

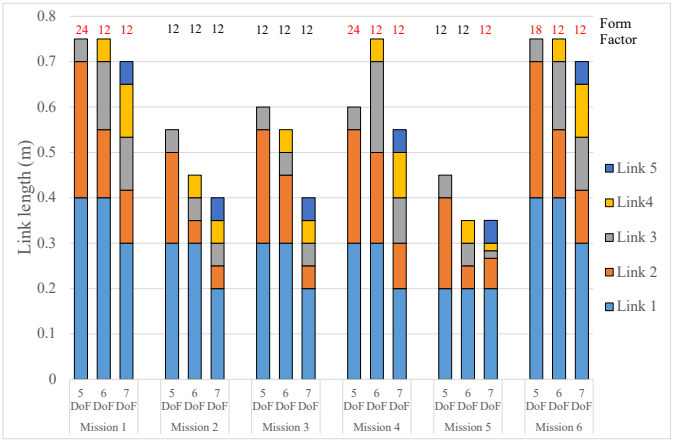

Fig. 4: Graph showing how the distribution of link lengths changes for each mission scenario dependent on the selected d.o.f. Also shown is the optimal form factor in each scenario. Form factors in red show the optimal system excluding the power analysis. This is because for these missions no base spacecraft could provide sufficient power, instead a battery will supplement these missions.

The power consumption is only shown for the missions in which sufficient power is available. It was thought that the higher d.o.f. manipulators would require more power. This is due to the increased number of joints and the more complex system applying increased reaction forces to the base. However, it can be seen that in missions 2, 3 and 5, the 5 d.o.f. system requires the highest power and the 7 d.o.f. system the lowest. This is attributed to the fact that the 5 d.o.f. manipulator is longest, and the 7 d.o.f. is the shortest. When the payload is further from the system's c.o.m larger forces are applied to the base spacecraft. This puts a higher demand on the AOCS, thus increasing power consumption. The longer link lengths also have higher inertia meaning that the actuators in the arm must apply larger forces, therefore increasing the power demands further.

E. Future Work

At this stage, the Ta-DAH Design toolbox has some limitations. The system requires in-depth knowledge in relation to the mission scenario. This is because a top level mission, such as debris removal, must be broken down into initial and final positions. This is not an easy task and it has been shown that a slight variation in input can lead to a large variation in both the optimal design and output behavior. Future work should alter the system to optimise the design based on the

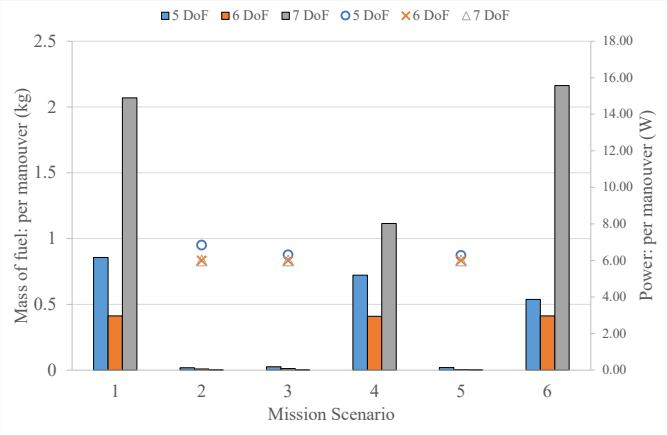

Fig. 5: Graph showing the fuel and power consumption for different missions, dependent on the d.o.f. of the manipulator. The bars represent the fuel consumption per manoeuvre for the different space robot designs. The scatter graph represents the power consumption per manoeuvre. The power required for missions 1, 4 and 6 are omitted from this graph since they exceed what is availabile from all form factors.

mission concept directly. Further improvements would be to include contact dynamics in the simulator model, and allow for a variation in the orbit used — currently all missions are run in GEO. In practice this orbit would vary depending on mission constraints and the operating condition (single agent vs multi agent) of the space robot. A variation in the orbit would lead to different power availability for the different form factors. In order to further advance the design process, and Ta-DAH Design's capability a method for streamlining the base and arm optimisation should be introduced. This will prevent the optimisation process from needing to be done in an iterative manner.

V. Conclusions

This paper presented Ta-DAH Design, an automated design process tailored to optimse the hardware of free-flying space robots. Designing a space robot is a challenging problem with many dimensions not present in terrestrial robotic design. However, the suitable design of such a system will have huge benefits in the industry via the automation of previously unattainable OOO, including OOA, ADR and other servicing missions.

The design process presented in this work uses a weighted cost function to optimise the link lengths of a robotic manipulator and then iterates over pre-defined form factors to optimise the size of the base spacecraft. The objective functions used in the cost function of the manipulator quantify a number of important performance parameters and are all defined and expanded in this work. The base spacecraft is sized by ensuring that the on-board subsystems can facilitate the manoeuvre required for any given task. Ta-DAH Design is implemented in a novel toolbox that has shown to provide an optimal space robot for an input mission in a maximum of 3 min. This is a drastic improvement over other approaches to robotic free-flying design, which rely on trial-and-error prototyping. In addition to this, Ta-DAH Design is a fully transparent process that is well documented and available for other engineers to use or adapt. It is believed that tools like this will revolutionise the way the space industry works, by allowing smaller entities, or new space companies, to leverage information from academia without needing to perform excessive R&D.

Appendix A
Joint Angles Used for Optimisation

	Mission		State Vector
5 d.o.f.	1	Start:	$0, 0, 0, 0, 0, 0, 0, 0, 0, 0, 0, 0$
		Final:	$1, -3, 2, 0, 0, 0, 0, 0, 30, 45, 0$
	2	Start:	$0, 0, 0, 0, 0, 0, 0, 0, 0, 0, 0$
		Final:	$0, 0, 0, 0, 0, 0, 0, 45, 0, 45, 90$
	3	Start:	$0, 0, 0, 0, 0, 0, 0, 0, 0, 0, 0$
		Final:	$0, 0, 0, 0, 0, 0, 30, 45, 50, 45, 0$
	4	Start:	$0, 0, 0, 0, 0, 0, 0, 0, 0, 0, 0$
		Final:	$1, -3, 2, 0, 0, 0, 30, -45, -30, -45, 90$
	5	Start:	$0, 0, 0, 0, 0, 0, 0, 0, 0, 0, 0$
		Final:	$0, 0, 0, 0, 0, 0, 45, 45, 30, 45, -90$
	6	Start:	$0, 0, 0, 0, 0, 0, 0, 0, 0, 0, 0$
		Final:	$1, -3, 2, 0, 0, 0, 40, -45, 0, -45, 0$
6 d.o.f.	1	Start:	$0, 0, 0, 0, 0, 0, 0, 0, 0, 0, 0, 0$
		Final:	$1, -3, 2, 0, 0, 0, 0, 0, 20, 30, 45, 0$
	2	Start:	$0, 0, 0, 0, 0, 0, 0, 0, 0, 0, 0, 0$
		Final:	$0, 0, 0, 0, 0, 0, 0, -30, 45, 0, 45, 90$
	3	Start:	$0, 0, 0, 0, 0, 0, 0, 0, 0, 0, 0, 0$
		Final:	$0, 0, 0, 0, 0, 0, 30, 20, 45, 50, 45, 0$
	4	Start:	$0, 0, 0, 0, 0, 0, 0, 0, 0, 0, 0, 0$
		Final:	$1, -3, 2, 0, 0, 0, 30, 0, -45, -30, -45, 90$
	5	Start:	$0, 0, 0, 0, 0, 0, 0, 0, 0, 0, 0, 0$
		Final:	$0, 0, 0, 0, 0, 0, 45, 30, 45, 30, 45, -90$
	6	Start:	$0, 0, 0, 0, 0, 0, 0, 0, 0, 0, 0, 0$
		Final:	$1, -3, 2, 0, 0, 0, 40, -20, -45, 0, -45, 0$
7 d.o.f.	1	Start:	$0, 0, 0, 0, 0, 0, 0, 0, 0, 0, 0, 0, 0$
		Final:	$1, -3, 2, 0, 0, 0, 0, 0, 20, 0, 30, 45, 0$
	2	Start:	$0, 0, 0, 0, 0, 0, 0, 0, 0, 0, 0, 0, 0$
		Final:	$0, 0, 0, 0, 0, 0, 0, -30, -20, 45, 0, 45, 90$
	3	Start:	$0, 0, 0, 0, 0, 0, 0, 0, 0, 0, 0, 0, 0$
		Final:	$0, 0, 0, 0, 0, 0, 30, 45, 20, 45, 50, 45, 0$
	4	Start:	$0, 0, 0, 0, 0, 0, 0, 0, 0, 0, 0, 0, 0$
		Final:	$1, -3, 2, 0, 0, 0, 30, 0, 20, -45, -30, -45, 90$
	5	Start:	$0, 0, 0, 0, 0, 0, 0, 0, 0, 0, 0, 0, 0$
		Final:	$0, 0, 0, 0, 0, 0, 45, 30, 0, 45, 30, 45, -90$
	6	Start:	$0, 0, 0, 0, 0, 0, 0, 0, 0, 0, 0, 0, 0$
		Final:	$1, -3, 2, 0, 0, 0, -45, 40, -20, -45, 0, -45, 0$

Acknowledgment

This work was partially supported by Surrey Satellite Technology Ltd and the UK Engineering and Physical Sciences Research Council (EPSRC) grant agreement EP/S035761/1 'Reflexive Robotics'.

REFERENCES

[1] Robotic manipulation and capture in space: A survey. *Frontiers in Robotics and AI*, 8, 2021.

[2] Ajith Abraham and Lakhmi C. Jain. Evolutionary multiobjective optimisation. In *Evolutionary Multiobjective Optimisationm Theoretical Advances and Applications*, pages 1–6. 2006.

[3] Hatem Al-Dois, A. K. Jha, and R. B. Mishra. Task-based design optimization of serial robot manipulators. *Engineering Optimization*, 45(6):647–658, August 2012.

[4] Simone Battistini, Chantal Cappelletti, and Filippo Graziani. An attitude determination and control system for a nano-satellite alternative launch platform. In *Proc. 67th International Astronautical Congress*, Guadalajara, Mexico. 26-30, September 2016.

[5] Bradford. Reaction wheel unit datasheet. URL, http://bradford-space.com/products-aocs-reaction-wheel-unit.php. Date Accessed 22/08/2019.

[6] Luca Carlone and Carlo Pinciroli. Robot co-design: Beyond the monotone case. In *International Conference on Robotics and Automation (ICRA)*, Montreal, Canada. 20-24, May 2019.

[7] Carlos A. Coello Coello. A comprehensive survey of evolutionary-based multiobjective optimization techniques. *Knowledge and Information Systems*, 1(3):269–308, 1999.

[8] Carlos A. Coello Coello. Twenty years of evolutionary multi-objective optimization: A historical view of the field. *IEEE Computational Intelligence Magazine*, 1(1):28–36, 2006.

[9] S Dahbi, A Aziz, S Zouggar, N Benazzi, H Zahboune, and M Elhfyani. Design and sizing of electrical power source for a nanosatellite using photovoltaic cells. In *Proc. 3rd IEEE International Renewable Sustainable Energy Conference*, Isreal. 10-13, December 2015.

[10] Thomas J. Debus and Sean P. Dougherty. Overview and performance of the front-end robotics enabling near-term demonstration (FREND) robotic arm. In *Proc. AIAA Infotech @Aerospace Conference*, Seattle, Washington. 6-9, April 2009.

[11] M. A. Difftler, T. D. Ahlstrom, R. O. Ambrose, N. A. Radford, C. A. Joyce, N. De La Pena, A. H Parsons, and A. L. Noblitt. Robonaut 2 - initial activities on-board the ISS. In *Proc. 2012 IEEE Aerospace Conference*, pages 1–12, Big Sky, MT. 3-10, March 2012.

[12] William R. Doggett, John T. Dorsey, Thomas C. Jones, and Bruce King. Development of a tendon-actuated lightweight in-space MANipulator (TALISMAN). In *Proc. 42nd Aerospace Mechanisms Symposium*, volume 405, NASA Goddard Space Flight Center. 14-16, May 2014.

[13] S. Dubowsky and E. Papaopoulos. The kinematics, dynamics and control of free-flying and free-floating space robotic systems. *IEEE Transactions on Robotics and Automation*, 9(5):531–543, 1993.

[14] Michael T. M. Emmerich and André H. Deutz. A tutorial on multiobjective optimization: fundamentals and evolutionary methods. *Natural Computing*, 17(3):585–609, 2018.

[15] Angel Flores-Abad, Ou Ma, Khanh Pham, and Steve Ulrich. A review of space robotics technologies for on-orbit servicing. *Progress in Aerospace Sciences*, 68:1–26, July 2014.

[16] Robert B. Friend. Orbital express program summary and mission overview. In *Proc. SPIE Defense and Security Symposium*, volume 6958, Orlando, Florida, USA. 15, April 2008.

[17] Clement M. Gosselin. The optimum design of robotic manipulators using dexterity indicies. *Robotics and Autonomous Systems*, 9(4):213–226, 1992.

[18] G. Herzinger, B. Brunner, R. Lampariello, K. Landzettel, J. Schott, and B. M. Steinmetz. Advances in orbital robotics. In *Proc. 2000 IEEE International Conference on Robotics and Automation*, volume 1, San Francisco, CA. 24-28, April 2000.

[19] Honeybee. Microsat CMG attitude control array datasheet. URL, https://honeybeerobotics.com/wp-content/uploads/2014/03/Honeybee-Robotics-Microsat-CMGs.pdf. Date Accessed 22/08/2019.

[20] Lucy Jackson, Chakravarthini M. Saaj, Asma Seddaoui, Calem Whiting, Steve Eckersley, and Simon Hadfield. Downsizing an orbital space robot: A dynamic system based evaluation. *Advances in Space Research*, 65(10):2247–2262, May 2020.

[21] Tuomo Kivela, Jouni Mattila, and Jussi Puura. A generic method to optimize a redundant serial robotic manipulator's structure. *Automation in Construction*, 81:172–179, 2017.

[22] S. Kucuk and Z. Bingul. Robot workspace optimization based on a novel local and global performance indicies. In *Proc. of the IEEE Symposium on Industrial Electronics*, Dubrovnik, Croatia. 20-23, June 2005.

[23] Jet Propulsion Laboratory. Mars 2020 perseverance landing press kit. Technical report, January 2020.

[24] Wei-Jie Li, Da-Yi Cheng, Xi-Gang Liu, Yao-Bing Wang, Wen-Hua Shi, Zi-Xin Tang, Feng Gao, Fu-Ming Zeng, Hong-You Chai, Wen-Bo Luo, Qiang Cong, and Zhen-Liang Gao. On-orbit service (OOS) of spacecraft: A review of engineering developments. *Progress in Aerospace Sciences*, 108:32–120, July 2019.

[25] Marc Manz, Sebastian Bartsch, Romain Caujolle, Torsten Vogel, Mark Shielton, Elie Allouis, Stefan Gornig, Francisco Javier Colmenero, Sebastian Torralbo, Marko Jankovic, Wiebke Brinkmann, Isabel Soto, Gonzalo Guerra, Daniel Silveira, Serra Carolina, Björn Ordoubadian, Eric Bertels, Jeremi Gancet, Pierre Letier, Manfred Doermer, and Stéphane Estable. Robotic architecture and operational concept for in-space assembly and servicing missions. In *16^{th} Symposium on Advanced Space Technologies in Robotics and Automation (ASTRA 2022)*, ESTEC Noordwijk, The Netherlands. 1–2, June 2022.

[26] R.T Marler and J.S Arora. Survey of multi-objective optimization methods for engineering. *Structural and Multidisciplinary Optimization*, 26(6):369–395, April 2004.

[27] Nanoavionics. Reaction wheels system 'SatBus 4RWO' datasheet. URL, https://n-avionics.com/subsystems/cubesat-reaction-wheels-control-system-satbus-4rw/. Date Accessed 22/08/2019.

[28] M Oda. Space robot experiments on NASDA's ETS-VII satellite - preliminary overview of the experiment results. In *IEEE International Conference on Robotics and Automation*, volume 1-4, pages 1390–1395, Detroit, MI, USA. 10-15, May 1999.

[29] A. P. Pashkevich and P.J. Flemming. A multiobjective optimisation approach to robotic manipulator design. In *IFAC Procedings Volumes*, volume 24, pages 387–392. July 1991.

[30] Maximo Roa, Korbinian Nottensteiner, Armin Wedler, and Gerhard Grunwald. Robotic technologies for in-space assembly operations. In *Proc. ESA 14^{th} Symposium on Advanced Space Technologies In Robotics and Automation (ASTRA)*, Leiden, The Netherlands. 20-22, June 2017.

[31] RockwellCollins. RSI 12 momentum and reaction wheels datasheet. URL, https://www.rockwellcollins.com/Products-and-Services/Defense/Platforms/Space/RSI-12-Momentum-and-Reaction-Wheels.aspx. Date Accessed 22/08/2019.

[32] Gordon Roesler, Paul Jaffe, and Glen Henshaw. Orbital mechanics. *IEEE Spectrum*, 54(3):44–50, March 2017.

[33] Timothy E. Rumford. Demonstration of autonomous rendezvous technology (DART) project summary. In *Proc. Volume 5088, Space Systems Technology and Operations*, volume 5088, Orlando, Florida, USA. 21-25, April 2003.

[34] Mine Sarac, Massimiliano Solazzi, Edoargo Sotgiu, Massimo Bergamasco, and Antonio Frisoli. Design and kinematic optimization of a novel underactuated robotic hand exoskeleton. *Meccanica*, 52(3):749–761, 2017.

[35] Asma Seddaoui, Chakravarthini Mini Saaj, and Manu Harikrishnan Nair. Modeling a controlled-floating space robot for in-space services: A beginner's tutorial. *Frontiers in Robotics and AI*, 2021.

[36] Y. Umetani and K. Yoshida. Workspace and manipulability analysis of space manipulators. *Transactions of the Society of Instument and Control Engineers*, 1(1):116–123, 2001.

[37] Tethers Unlimited. Kracken^{TM} robotic arm data sheet. Technical report, 2018.

[38] Vacco. CuSP propulstion system. URL, https://www.cubesat-propulsion.com/cusp-propulsion-system/. Date Accessed 27/08/2019.

[39] Vacco. AFRL propulsion unit for cubesats. URL, https://www.cubesat-propulsion.com/propulsion-unit/. Date Accessed 27/08/2019.

[40] Vacco. NASA C-POD micro cubesat propulsion system data sheet. URL, https://www.cubesat-propulsion.com/reaction-control-propulsion-module/. Date Accessed 23/08/2019.

[41] Dan Zhang and Bin Wei. Modelling and optimisation of a 4 DoF hybrid robotic manipulator. *International Journal of Computer Integrated Manufacturing*, 30(11):1179–1189, 2017.